View metadata, citation and similar papers at core.ac.uk

brought to you by CORE

provided by Archivio della ricerca- Università di Roma La Sapienza

MNRAS **454,** 2677–2690 (2015) doi:10.1093/mnras/stv2123

High-velocity stars from close interaction of a globular cluster and a supermassive black hole

R. Capuzzo-Dolcetta★ and G. Fragione★

Dept. of Physics, Sapienza, Univ. of Roma, P.le A. Moro 2, I-00185 Roma, Italy

Accepted 2015 September 9. Received 2015 September 4; in original form 2015 July 23

ABSTRACT

Observations show the presence, in the halo of our Galaxy, of stars moving at velocities so high to require an acceleration mechanism involving the presence of a massive central black hole. Thus, in the frame of a galaxy hosting a supermassive black hole (10^8 $M_\odot$) we investigated a mechanism for the production of high-velocity stars, which was suggested by the results of *N*-body simulations of the close interaction between a massive, orbitally decayed, globular cluster and the supermassive black hole. The high velocity acquired by some stars of the cluster comes from the transfer of gravitational binding energy into kinetic energy of the escaping star originally orbiting around the cluster. After the close interaction with the massive black hole, stars could reach a velocity sufficient to travel in the halo and even overcome the galactic gravitational well, while some of them are just stripped from the globular cluster and start orbiting on precessing loops around the galactic centre.

Key words: stars: kinematics and dynamics – galaxies: haloes – galaxies: nuclei – galaxies: star clusters: general.

1 INTRODUCTION

The existence of high-velocity stars in the Galactic halo is an ascertained feature. Some of them have speed sufficient to escape the Galaxy gravitational potential. They may have gained such high velocities thanks to different physical mechanisms, as three-body interactions among binary systems in star clusters or with the massive black hole (BH) in the Galactic Centre. High-velocity stars can be divided in two different categories, i.e. runaway stars and hypervelocity stars (HVSs).

Runaway stars, historically defined in the context of O and B stars (Humason & Zwicky 1947), are Galactic halo stars with peculiar motions higher than 40 km s^{-1} (although the definition of runaway star is not univocal). Young massive stars are not expected to be observed in the halo far from star-forming regions, since special conditions, as the presence of molecular clouds with dense cores, are required to form such stars. Therefore, they are thought to be born not in the halo, but rather to have travelled far from their birthplace. There are two proposed mechanisms for the production of runaway stars: supernova ejections and dynamical ejections (Silva & Napiwotzki 2011).

In the supernova ejection mechanism (Blaauw 1961; Portegies Zwart 2000) a runaway star is supposed to have origin in a binary system when its companion explodes as a supernova. The maximum possible ejection velocity is given by the sum of the orbital velocity of the progenitor binary and of the supernova kick velocity. Additional effects may come from asymmetric explosions (Scheck et al. 2006; Przybilla et al. 2008), but, in any case, runaways velocities are below the Galactic escape velocity. In the dynamical ejection mechanism (Poveda, Ruiz & Allen 1967) the runaway star derives from a three- or four-body interaction. For example, if a binary system interacts with a massive star, one member of the binary could be captured by the massive star, while the other star may be ejected with high velocity (Leonard & Duncan 1990; Gvaramadze 2009; Gvaramadze, Gualandris & Portegies Zwart 2009; Gvaramadze & Gualandris 2011; Perets & Subr 2012). In this case, the maximum possible ejection velocity is the escape velocity of the most massive star. Observations show that both the ejection mechanisms operate in nature (Hoogerwerf, de Bruijne & de Zeeuw 2001).

HVSs are stars escaping the host Galaxy. Hills (1988) was the first to predict theoretically their existence as a consequence of interactions with a massive BH in the Galactic Centre, while Brown et al. (2005) serendipitously discovered the first HVS in the outer stellar halo, a B-type star moving over twice the Galactic escape velocity. The most recent HVS Survey is the MMT (Multiple Mirror Telescope) survey, a spectroscopic survey of stars within the range of colours of 2.5–4-$M_\odot$ late B-type stars (Brown, Geller & Kenyon 2014). The MMT observational approach is justified by the fact that such stars should not exist at faint magnitudes in the outer halo unless they were ejected until those distances. Actually, such stars have relatively short lifetimes and should originate in a region of ongoing star formation. The MMT survey revealed 21 HVSs ejected from the Milky Way (MW) at distances between 50 and 120 kpc. However, the MMT survey is able to measure only the component

★ E-mail: roberto.capuzzodolcetta@uniroma1.it (RCD); giacomo.fragione@uniroma1.it (GF)

© 2015 The Authors
Published by Oxford University Press on behalf of the Royal Astronomical Society

Downloaded from http://mnras.oxfordjournals.org/ at Universita' degli Studi Roma La Sapienza on May 6, 2016

along the line of sight of the velocity vector. To compute the other velocity components, a measure of proper motions is needed. This is in most of the cases not possible (but for some special cases; Brown et al. 2010), because HVSs found by MMT Survey are very distant so that their proper motions are too small ($\leq$1 mas yr^{-1}) to be measured with ground-based telescopes. Moreover, as said above, the MMT Survey is biased to the observation of stars within the colour range of 2.5–4-M$_\odot$ late B-type stars, although an observational effort to find an older population of HVSs (Brown, Geller & Kenyon 2009; Kollmeier et al. 2009, 2010) has been done, unsuccessfully, in the last years.

Hills' mechanism involves the tidal break-up of a binary passing close to a massive BH. This mechanism was analysed by other authors in the attempt to shed light on the properties of the stars that are accelerated in such a way (Yu & Tremaine 2003; Gualandris, Portegies Zwart & Sipior 2005; Bromley et al. 2006; Sari, Kobayashi & Rossi 2009; Kobayashi et al. 2012; Rossi, Kobayashi & Sari 2014). The tidal break-up of a binary could lead also to a population of stars orbiting in the inner regions of the Galaxy around the central BH, the so-called S stars (Gould & Quillen 2003; Ginsburg & Loeb 2006; Perets, Hopman & Alexander 2007). Since the Hills prediction, a lot of other mechanisms have been proposed in the literature to explain the production of high-velocity and hypervelocity stars, which involve different astrophysical frameworks and phenomena (Tutukov & Federova 2009).

(i) The interaction of a supermassive black hole (SMBH) binary with a single star in the nucleus of the host galaxy. In this way stars can be accelerated at velocities high enough to escape the local gravitational potential (Gualandris et al. 2005; Baumgardt, Gualandris & Portegies Zwart 2006; Sesana, Haardt & Madau 2006).

(ii) Some stars can come from another (nearby) galaxy with a high velocity relative to the present galactic environment (Gualandris & Portegies Zwart 2007; Bonanos et al. 2008; Sherwin, Loeb & O'Leary 2008; Perets 2009; Brown et al. 2010).

(iii) The close encounter of a hard massive binary star and a single massive star could produce stars with velocities larger than the local escape velocity (Gvaramadze et al. 2009).

(iv) A supernova explosion in a close binary can give a kick to the companion to accelerate it to a very high velocity (Portegies Zwart 2000; Zubovas, Wynn & Gualandris 2013).

An interesting point is that, as shown by Hansen (2007) and Lopez-Morales & Bonanos (2008), HVSs in our Galaxy have both slow and rapid rotations, suggesting different acceleration mechanisms. Note indeed that HVSs originated by a binary disrupted by a BH are not expected to be fast rotators and so this origin is unlikely for fast rotating HVSs. Therefore, since HVS production mechanisms should involve different astrophysical frameworks and phenomena, it would be possible to infer information about different pieces of physics, as that of the three-body interaction, the physics of the region near massive BHs (Gould & Quillen 2003; Sesana, Haardt & Madau 2007; O'Leary & Loeb 2008) as well as the physics of supernovae. Moreover, the study of the proper motions of such fast-moving stars can improve the knowledge of the Galaxy gravitational potential shape, of its dark matter component (Gnedin et al. 2005; Yu & Madau 2007) and, in line of principle, may lead to useful information also for cosmology (Loeb 2011).

Observations of high-velocity and hypervelocity objects have been limited to high-mass, early-type stars due to obvious observational bias. Observers have started investigating low-mass high-velocity stars only recently (Palladino et al. 2014; Zhong et al. 2014; Li et al. 2015; Vickers, Smith & Grebel 2015), some of which are low-mass HVS candidates. The European Space Agency satellite *Gaia*[1] is expected to measure proper motions with a precision of 0.1 mas yr^{-1} and so will be able to provide for a larger and less biased sample. Furthermore, *Gaia* is expected to find $\sim$100 HVSs in a sample of $\sim 10^9$ stars.

Table 1. The values of α, the eccentricity e, the pericentre r_- and apocentre r_+ of the GC elliptical orbits.

α	e	r_-(pc)	r_+(pc)
0.1	0.95	0.51	19.6
0.2	0.89	1.06	18.9
0.3	0.84	1.63	18.5
0.4	0.77	2.25	17.8
0.5	0.71	2.93	17.1

The aim of this paper is to investigate another mechanism of production of high-velocity stars, which involves a globular cluster (GC) that during its orbit has the chance to pass close to an SMBH in the centre of its host galaxy. This chance is increased by the orbital decay suffered by massive clusters moving a dense galactic environment, which makes significant the dynamical friction braking exerted by the stars of the galaxy (Capuzzo-Dolcetta 1993; Capuzzo-Dolcetta & Miocchi 2008; Antonini et al. 2012). For the test cases of this paper, we assumed $M_{\rm BH} = 10^8\,{\rm M}_\odot$ with the scope of better identifying the underlying physical mechanism.

The paper is organized this way: in Section 2 we outline and describe our approach to the study of the consequences of the GC–SMBH interaction; in Section 3 the results are presented and discussed; in Section 4 we draw the conclusions. Significant details are given in the appendix.

2 METHOD

Our scattering experiments refer to the interaction of three different bodies: an SMBH, a GC and a star. In our simulations the SMBH sits initially in the origin of the reference frame, while the GC follows an elliptical orbit at a relatively close distance around it. The assumption of close distance to the BH is motivated by the fact that the GC is supposedly orbitally decayed by dynamical friction braking, as discussed in Arca Sedda et al. (in preparation). Given the BH influence radius as that within which the BH potential dominates

$$r_{\rm inf} = \frac{G M_{\rm BH}}{\sigma^2}, \qquad (1)$$

where σ is the star's velocity dispersion in the central galactic region, we can treat the dynamics of the star interacting with the environment as a three-body (GC, SMBH and test star around the GC) problem whenever the relevant fly-by passage occurs within the distance $r_{\rm inf}$ from the SMBH. In the cases studied in this paper (Section 3), $r_{\rm inf} \lesssim 12.5$ pc, which means that the choice we make in this paper of 10 pc as radius of the GC circular reference orbit, with the values of pericentres distances (around which the scattering is effective) given in Table 1, is fully compatible with the neglect of the smooth external field.

[1] http://www.cosmos.esa.int/web/gaia

Downloaded from http://mnras.oxfordjournals.org/ at Universita' degli Studi Roma La Sapienza on May 6, 2016

Actually, neglecting the stellar background potential, the mechanical energy (per unit mass) of the GC on a circular orbit of radius r_c is

$$E_c \equiv \frac{1}{2}v_c^2 - \frac{GM_{BH}}{r_c} = -\frac{1}{2}\frac{GM_{BH}}{r_c}, \quad (2)$$

given that the circular velocity is $v_c = (GM_{BH}/r_c)^{1/2}$. Consequently, taking into account that the angular momentum per unit mass of the GC on the circular orbit around the BH is $L_c = \sqrt{GM_{BH}r_c}$, the pericentre (r_-) and apocentre (r_+) distances of the GC on orbits of same energy (E_c) but different angular momentum $0 \le L \le L_c$ are given by

$$r_\pm = r_c\left(1 \pm \sqrt{1 - \left(\frac{L}{L_c}\right)^2}\right). \quad (3)$$

Of course in the above equation the $-$ sign gives the pericentre and the $+$ sign gives the apocentre. In conclusion, once we have, as reference, a circular orbit of radius r_c we may compare it with a set of orbits at same energy just varying the ratio L/L_c. The eccentricity of the orbit is, trivially,

$$e = \frac{r_+ - r_-}{r_- + r_+} = \sqrt{1 - \left(\frac{L}{L_c}\right)^2}. \quad (4)$$

We varied the parameter

$$\alpha \equiv \left(\frac{L}{L_c}\right)^2, \quad (5)$$

in order to sample GC orbits of different eccentricity and same orbital energy. Of course, $\alpha = 0$ for radial orbits ($e = 1$) and $\alpha = 1$ for circular orbits ($e = 0$).

The Cartesian reference frame has been chosen as that with the x-axis along the line connecting the GC with the SMBH and y-axis orthogonal, so that the (x, y) frame is equiverse to the GC orbital revolution.

In the restricted three-body problem, the existence of the Hills surfaces which enclose the two finite-mass bodies (Szebehely 1966) is well known. The radius of the Hills sphere, given by

$$r_L = r_0\left(\frac{M_{GC}}{3M_{BH}}\right)^{1/3}, \quad (6)$$

defines the spherical volume around the GC where its gravitational potential dominates. Outside the Hills sphere, the BH potential overcomes the one of the cluster. For the set of parameters used in our scattering experiments, $0.55 \le r_L \le 0.63$ pc, $1.19 \le r_L \le 1.36$ pc and $2.55 \le r_L \le 2.93$ pc for a GC of mass 10^4, 10^5 and 10^6 $M_\odot$, respectively.

A meaningful study refers to the fate of stars moving around the GC with orbits initially all within the GC influence radius. Therefore, we put the initial circular orbits, on which the test star moves around the GC, inside this sphere by setting the radius of this orbit to be a fraction (<1) of the distance from the first Lagrange point (L1) and the GC.

For the sake of statistical significance, once fixed, the unperturbed star circular orbit, we sampled cases with initial different phases, in the range 0°–360° at increments of 15° (Ginsburg, Loeb & Wegner 2012).

To summarize, in this paper the values of the relevant initial parameters have been set as follows (see also Table 1):

(i) the SMBH mass is $M_{BH} = 10^8$ $M_\odot$;

(ii) the GC mass, M_{GC}, assumes the three values 10^4, 10^5 and 10^6 $M_\odot$;

(iii) the test star mass, m_*, is set equal to 1 $M_\odot$;

(iv) the GC reference circular orbit has the radius $r_0 = 10$ pc;

(v) the GC orbital eccentricity ranges from $e = 0.71$ ($\alpha = 0.5$) to $e = 0.95$ ($\alpha = 0.1$) and is parametrized varying $0.1 \le \alpha \le 0.5$ at steps of 0.1;

(vi) the test star circular orbit radius around the GC is parametrized by $\beta \equiv r/r_L$, whose values are in the range 0.08–0.25;

(vii) the star initial position on the circular orbit of given radius (see above) is parametrized by adopting a set of 24 different angles spanning 0°–360° with a 15° step;

(viii) the star circular orbit around the GC and the GC orbit with respect to the BH are coplanar.

The choice of the range of α, and consequently of e, towards large values of e, is due to the fact that (as we will see in Section 3) the efficiency of the energy transfer on the test star orbiting the GC tends to vanish at eccentricities less than ∼0.6.

Given the above set of initial parameters, we integrated the system of the differential equations of the three-body (SMBH, GC and star) motion,

$$\ddot{\boldsymbol{r}}_i = -G\sum_{j\neq i}\frac{m_j(\boldsymbol{r}_i - \boldsymbol{r}_j)}{\left|\boldsymbol{r}_i - \boldsymbol{r}_j\right|^3}, \quad (7)$$

for $i = 1, 2, 3$, using the fully regularized algorithm of Mikkola & Aarseth (2001). The need of a regularized algorithm is due to the enormous range of variation of the masses involved, going from 1 $M_\odot$ of the test star to 10^8 $M_\odot$ of the SMBH. Any not-regularized direct summation code would fail in dealing with the close star–SMBH interaction and would carry to an enormous energy error during the close triple encounter.

In Mikkola's ARW code this problem is overcome by a transformed leapfrog method, which leads to extremely accurate integrations of the bodies trajectories when combined with the Bulirsch–Stoer extrapolation method (Bulirsch & Stoer 1966; Mikkola & Tanikawa 1999a,b; Mikkola & Merritt 2006, 2008; Hellström & Mikkola 2010). Thanks to the regularized algorithm, the fractional energy error is kept below 10^{-11} over the whole integration time.

3 RESULTS

In our scattering experiments the test star orbiting the GC has three possible fates:

(1) it remains bound to the GC on an orbit significantly perturbed respect to the original one;

(2) it becomes a *high-velocity* star, either bound or unbound to the host galaxy;

(3) it is captured by the massive BH gravitational field and starts revolving around it.

The distinction among these three different situations is made by computing the mechanical energy of the star respect to the BH and the GC after the scattering. If the energy of the star with respect to the GC remains negative, the star remains bound to the GC; if this energy becomes positive, while the star energy with respect to the BH is negative, the star becomes bound to the BH. Finally, if both these energies are positive, the star is able to leave the BH–GC system and, according to the assumed galactic potential model, it will be bound or unbound respect to the galaxy. The branching ratios,

Downloaded from http://mnras.oxfordjournals.org/ at Universita' degli Studi Roma La Sapienza on May 6, 2016

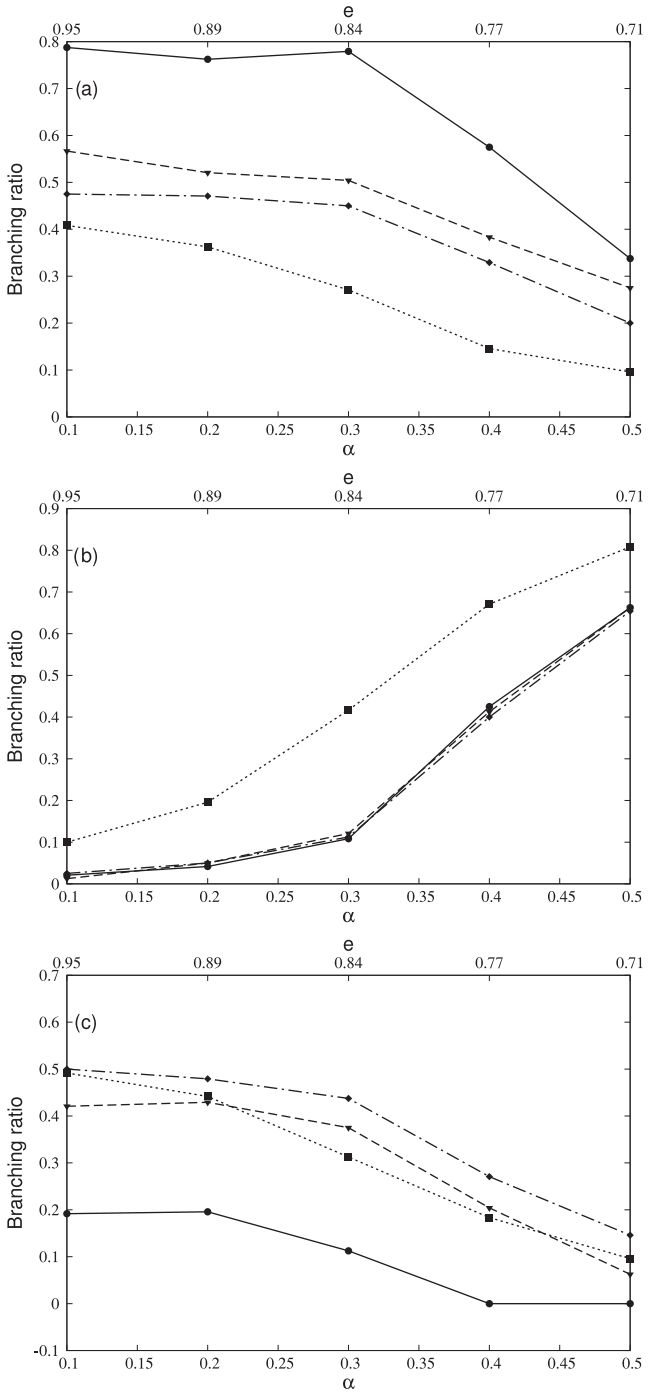

Figure 1. Branching ratios of stars captured by the BH (a), GC stars (b) and ejected stars (c), after GC–BH scattering, for $M_{\rm GC} = 10^4\,{\rm M}_\odot$ (solid line), $M_{\rm GC} = 10^5\,{\rm M}_\odot$ (dashed line), $M_{\rm GC} = 10^6\,{\rm M}_\odot$ (dot–dashed line) and different GC orbits, parametrized by $\alpha = (L/L_{\rm c})^2$. The dotted lines represent the branching ratios when the star orbit and GC orbit are perpendicular for $M_{\rm GC} = 10^6\,{\rm M}_\odot$.

i.e. the probability of different outcomes, are plotted in Figs 1(a), (b) and (c).

Fig. 1(a) gives the branching ratio of stars which are captured by the BH after the GC–BH scattering and become bound to the BH, as function of α for the different GC masses. As expected, this ratio decreases for larger values of α (less eccentric orbits), as well as for larger GC masses.

Fig. 1(b) shows the branching ratio of stars which remain gravitationally bound to the GC after GC–BH scattering, as function of α for the different GC masses. The branching ratio increases for higher values of α, i.e. for less eccentric orbits, and is almost independent of the GC mass in the range studied. Note that at values of $e \sim 0.7$ the fraction of bound stars is about 80 per cent for the $10^4\,{\rm M}_\odot$ GC and about 67 per cent for the 10^5 and $10^6\,{\rm M}_\odot$ cases.

Finally, Fig. 1(c) shows the branching ratio of stars which, after GC–BH scattering, leave the BH–GC system becoming high-velocity stars, as function of α for the different GC masses. This fraction decreases for larger values of α (less eccentric orbits) and increases for larger GC masses.

The Lagrangian radii have an important role during the close interaction between GC and BH. A star is lost by the GC when it crosses the Hills surface through or near the first or the second Lagrangian point. If it passes through L1, its fate is the capture by the BH, while in the second case it will escape the whole system, becoming unbound both with respect to the BH and the GC. The first channel is favoured by lower GC to BH mass ratios, since the BH potential is stronger and is able to capture a higher number of GC stars making them pass through the first Lagrangian point. At the same time, the GC gravitational potential is not so intense to give the star a velocity high enough to escape the whole GC–BH system. Therefore, the branching ratio for the production of stars captured by the BH is higher for lower GC masses, while the branching ratio of ejected stars increases for higher GC masses.

Another important feature of this mechanism is the significant level of collimation of the ejected stars. Fig. 2(a) shows the average ejection angle ϕ as function of α for different GC masses. This angle is that between the velocity vector at ejection and the x-axis of the inertial reference frame, taken in the direction pointing from the BH to the initial position of the GC. Fig. 2(b) shows the ratio between the standard deviations σ_ϕ and ϕ, giving a measure of the ejection collimation. If the value of σ_ϕ was precisely zero, it would mean that all the stars are ejected along the same direction after the GC–BH interaction. Therefore, non-zero values measure the width of the loss-cone within which stars are ejected. We see that the average emission angle increases for larger values of the GC mass, while the level of collimation decreases. Therefore, stars ejected during the interaction of a low-mass GC and a massive BH are concentrated in a small amplitude jet, which, instead, has a greater span for a high-mass GC. These results are compatible with Sesana et al. (2006), who found, studying the HVS production of a binary BH, that the collimation is higher when the mass ratio between the BHs is lower. Actually, we found that stars are highly collimated in jets when $M_{\rm GC} = 10^4\,{\rm M}_\odot$, while for higher GC masses the ejection jets tend to become a nearly isotropic emission.

3.1 High-velocity stars

From our scattering experiments, it is possible to derive the velocity profile of the ejected stars. Fig. 3 shows the velocity profile of the ejected stars at 20 pc (as it will be justified in the following) for different GC masses and all the orbits. The distributions are nearly Gaussian, cut at 212 km s^{-1}, which is the escape velocity from the BH. Moreover, the peak of the distribution depends on the GC mass, the greater the velocity peak the larger the GC mass. The ejected stars can have two fates:

(1) to remain gravitationally bound to the galaxy, although having escaped the BH–GC system;

Downloaded from http://mnras.oxfordjournals.org/ at Universita' degli Studi Roma La Sapienza on May 6, 2016

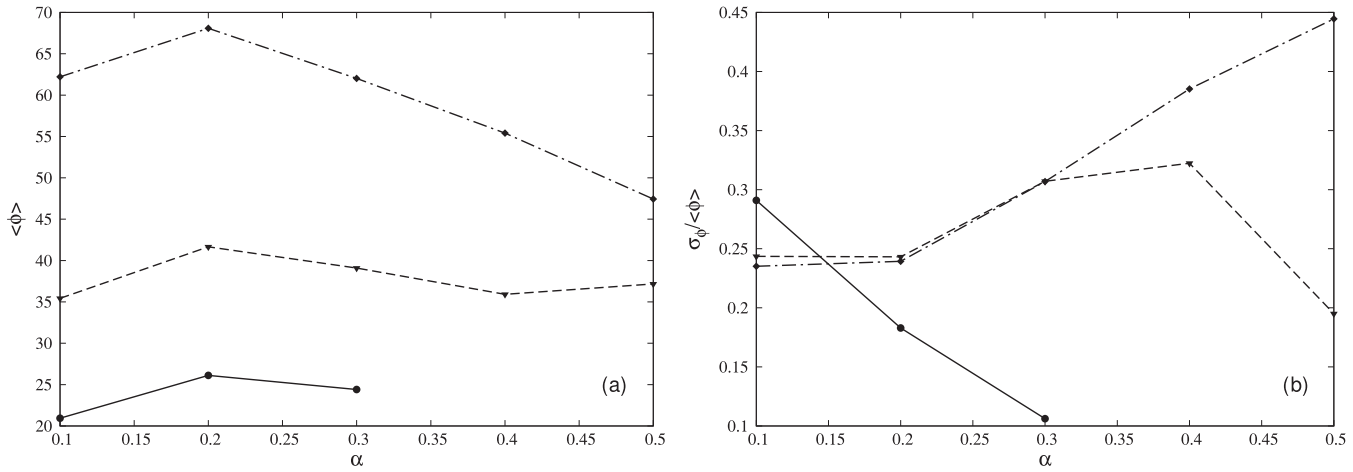

Figure 2. Average 'emission' angle of the ejected stars (a) and relative dispersion (b), both as function of α, for $M_{\rm GC} = 10^4\,{\rm M}_\odot$ (solid line), $M_{\rm GC} = 10^5\,{\rm M}_\odot$ (dashed line), $M_{\rm GC} = 10^6\,{\rm M}_\odot$ (dot–dashed line).

(2) to become unbound stars, and so HVSs, if their kinetic energy is sufficient to overcome the galaxy gravitational potential well.

To evaluate whether stars formerly belonging to the GC and ejected at high velocity remain bound to the host galaxy, an assumption on the galactic field has to be made. In our analysis, we assumed two different models for the host galaxy, one as an elliptical and one as a spiral galaxy.

The elliptical galaxy potential is represented as a two-component model given by a spherical bulge–halo summed to the SMBH potential. The bulge–halo potential is given by (Hernquist 1990)

$$\Phi_{\rm b}(r) = -\frac{GM_{\rm b}}{r + a_{\rm b}}, \tag{8}$$

where $M_{\rm b} = 7.8 \times 10^{10}\,{\rm M}_\odot$ and $a_{\rm b} = 5.4$ kpc. Note that these values are taken from Marconi & Hunt (2003) to represent the elliptical galaxy NGC 3377, whose central BH has an estimated mass $M_{\rm BH} = 1.0^{+0.9}_{-0.1} \times 10^8\,{\rm M}_\odot$.

Assuming the host galaxy as a spiral, we consider a four-component model for its potential

$$\Phi(r, z) = \Phi_{\rm BH}(r) + \Phi_{\rm b}(r) + \Phi_{\rm d}(r, z) + \Phi_{\rm h}(r), \tag{9}$$

where the indexes b, d and h stands for bulge, disc and halo, respectively. As above, the bulge potential is expressed as a Hernquist sphere (Hernquist 1990) with the constants $M_{\rm b} = 10^{10}\,{\rm M}_\odot$ and $a_B = 1$ kpc, as taken from Kornreich & Lovelace (2008) and Lingam (2014), to reproduce the parameters observed in giant disc galaxies such as those described by Wang, Sulkanen & Lovelace (1992) and Rownd, Dickey & Helou (1994).

The axisymmetric disc potential is (Miyamoto & Nagai 1975)

$$\Phi_{\rm d}(r, z) = -\frac{GM_{\rm d}}{\sqrt{r^2 + \left(a_{\rm d} + \sqrt{z^2 + b_{\rm d}^2}\right)^2}}, \tag{10}$$

where $M_{\rm d} = 10^{11}\,{\rm M}_\odot$, $a_{\rm d} = 6.5$ kpc and $b_{\rm d} = 0.26$ kpc (Lingam 2014).

Finally, the halo density distribution accounts for the presence of a spherical dark matter halo, of total mass $5.6 \times 10^{11}\,{\rm M}_\odot$, whose potential is (Binney 1981)

$$\Phi_{\rm h}(r) = \frac{1}{2} v_{\rm h}^2 \ln(r^2 + r_{\rm h}^2) + c, \tag{11}$$

where $v_{\rm h} = 250$ km s^{-1}, $r_{\rm h} = 2$ kpc and c is a constant which gives a match with an external ($r \geq 50$ kpc) keplerian potential (Fujita 2009; Lingam 2014).

Given a galaxy model, it is possible to calculate the escape velocity

$$v_{\rm esc}^{(j)}(r, z) = \sqrt{\sum_i -2\Phi_i(r, z)}, \tag{12}$$

which depends, besides on the galaxy model itself ($j = {\rm E, S}$), also on the position in which it is computed. In our three-body scattering, we follow the trajectories of stars until they are 20 pc far from the BH and compute their velocity and the escape velocity at this distance. At this distance the contribution of the galaxy components is not negligible in the equation (12), but its gravitational potential is nearly constant, both for the elliptical and spiral galaxy. Therefore, the motion of the escaping star is due to only the central BH.

If $v_* < v_{\rm esc}$, the star, although escapes the BH–GC system, will be gravitationally bound to the galaxy. In this case, the star can be bound only to some galactic components, as specified by the vertical lines in Fig. 3, which divide the distribution in different portions. The leftmost thick line in all the panels indicates the escape velocity from the BH (212 km s^{-1}). In the left-hand column panels, the other vertical line refers to the escape velocity (418 km s^{-1}) from the BH + bulge–halo system, while, in the right-hand column panels, the other vertical lines indicate the escape velocity with respect to the BH + bulge (365 km s^{-1}), BH + bulge + disc (516 km s^{-1}) and BH + bulge + disc + dark halo (759 km s^{-1}), respectively. Therefore, for example, the portion of velocity distribution, on the right of the 365 km s^{-1} vertical line (for a spiral galaxy), is unbound with respect to the BH + bulge component but bound with respect to the disc and the dark halo.

On the contrary, if $v_* > v_{\rm esc}$, it will become an HVS. The branching ratios of HVSs, i.e. the probability of producing unbound stars from the galaxy with respect to the total ejected stars, are listed in Table 2 for all the orbits. The results, which depend on both the total mass of the host galaxy and on the shape of its gravitational potential, show that the higher is the GC mass the higher is the probability of producing HVSs. Furthermore, according to the parameters chosen for the host galaxies gravitational potential, while the $10^6\,{\rm M}_\odot$ GC is able to generate HVSs in both the galaxies, the

Downloaded from http://mnras.oxfordjournals.org/ at Universita' degli Studi Roma La Sapienza on May 6, 2016

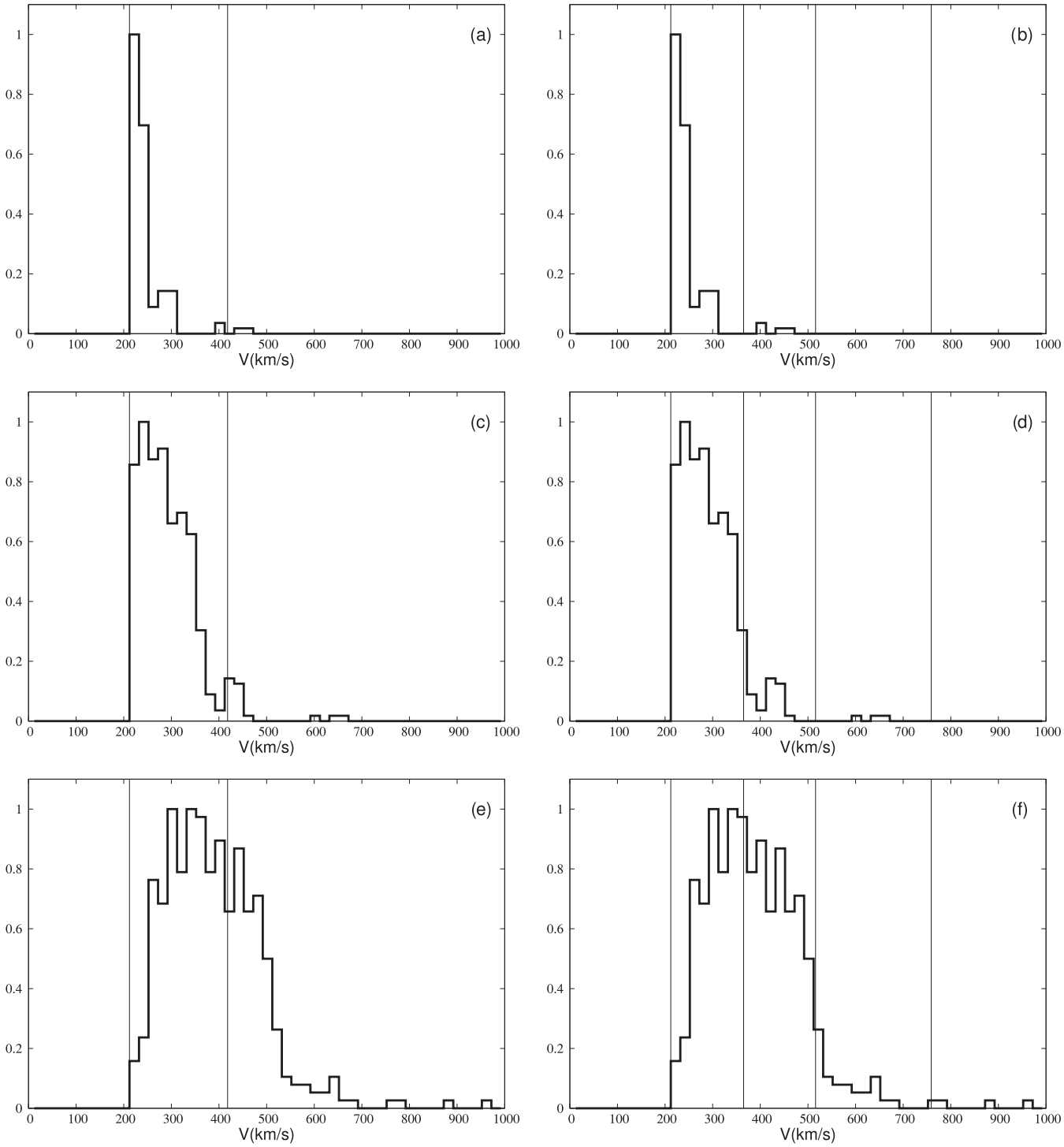

Figure 3. Velocity distribution of escaping stars for $M_{GC} = 10^4\,M_\odot$ (a, b), $M_{GC} = 10^5\,M_\odot$ (c, d) and $M_{GC} = 10^6\,M_\odot$ (e, f) and all the orbits, both for an $M_{tot} = 7.81 \times 10^{10}\,M_\odot$ elliptical galaxy (Marconi & Hunt 2003, left-hand column) and an $M_{tot} = 6.60 \times 10^{11}\,M_\odot$ spiral galaxy (Fujita 2009, right-hand column). Vertical lines indicate the escape velocity of the various galactic components (see Section 3.1).

10^4 and $10^5\,M_\odot$ GC are able to produce HVSs only in the elliptical galaxy.

3.2 The role of star orbital inclination

In our scattering experiments the initial orbit of the star and the orbit of the GC are coplanar. In order to check the effect of the relative inclination between the star and the GC orbit, we performed the same set of simulations for the $M_{GC} = 10^6$ GC presented above in the case of star orbits initially lying on a plane perpendicular to the GC orbital plane. The resulting branching ratios are plotted in Fig. 1. While the branching ratios of the ejected stars and of the stars captured by the BH decrease, the branching ratio of stars which remain bound to the GC increases. Therefore, the overall effect is

Downloaded from http://mnras.oxfordjournals.org/ at Universita' degli Studi Roma La Sapienza on May 6, 2016

Table 2. Branching ratio (third column) of the unbound stars (HVSs) with respect to the total ejected stars for different galaxy models (E = elliptical, S = spiral).

$M_{GC}(M_\odot)$	Galaxy	BR
10^4	E	1.67×10^{-2}
10^4	S	0
10^5	E	4.47×10^{-2}
10^5	S	0
10^6	E	0.35
10^6	S	9.09×10^{-3}

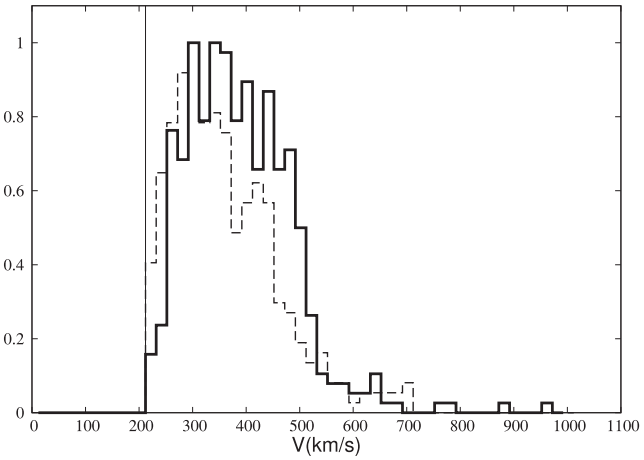

Figure 4. Comparison between the velocity distributions of escaping stars for $M_{GC} = 10^6\,M_\odot$ when the GC orbit and star orbit are coplanar (solid line) and when they are perpendicular (dashed line). The distributions are cut on the left-hand side at 212 km s^{-1}, which corresponds to the escape velocity with respect to the BH.

that stars tend to remain more bound to the cluster in the inclined case with respect to the coplanar one.

Fig. 4 shows the comparison of the velocity profiles. The perpendicularity of the orbits makes the distribution to peak at lower values of the velocity and the area under the distribution is smaller, because the branching ratio of ejected stars is lower than in the coplanar case.

3.3 The role of a smooth GC potential

In order to see the effect of a GC mass profile in the results, we performed the same set of simulations performed in the case of an $M_{GC} = 10^6$ point mass GC, assuming a Plummer (1911) mass profile

$$M(r) = M_{GC}\frac{r^3}{(r^2+a^2)^{3/2}}, \tag{13}$$

where M_{GC} is the total mass of the GC and a its core radius, which is set to 0.5 pc. Fig. 5 shows the velocity profiles for a point mass GC and a Plummer GC. The clear effect of smoothing the GC potential is that the velocity distribution shifts towards lower values of the velocity. Actually, for the set of parameters chosen in this study the gravitational energy of the star is $\sim GM_{GC}/a$, which leads the peak of the nearly Gaussian distribution to a lower velocity and makes its dispersion decrease. Actually, if the GC is taken to be a point mass, for same radius of the circular orbit, the generic star of our

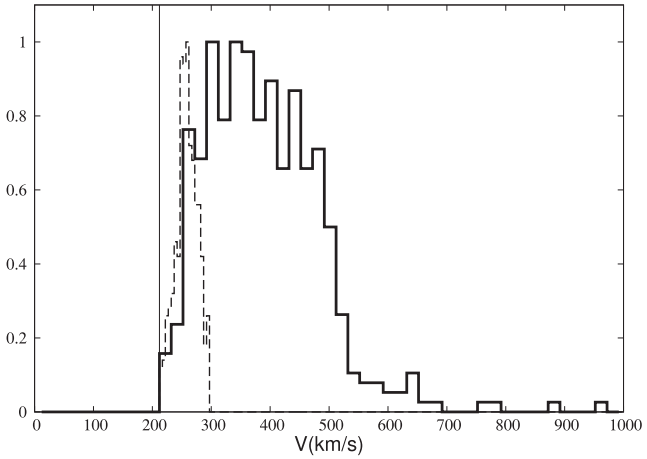

Figure 5. Comparison between the velocity distributions of escaping stars for $M_{GC} = 10^6\,M_\odot$ when the GC is approximated as a point mass (solid line) and when it has a Plummer density profile with core radius $a = 0.5$ pc (dashed line). The distributions are cut on the left-hand side at 212 km s^{-1}, which corresponds to the escape velocity with respect to the BH.

simulation has a lower (more tightly bound) gravitational energy with respect to the case of a GC smooth potential. Then the amount of gravitational energy that could be converted into kinetic energy would be higher, giving a larger number of ejected stars and a velocity distribution peaked at higher velocities. Clearly, this same effect of reduction of the efficiency in the star acceleration after the GC–MBH fly-by is obtained when the BH mass is reduced, reducing thus the quantity of gravitational energy to inject in the test star motion. This means that we would expect a scaling of the phenomenon efficiency almost linear with the MBH mass, which would mean a reduction of the effects studied in this paper, where the SMBH mass is $10^8\,M_\odot$, for a factor 0.04 in the case of the MW $4 \times 10^6\,M_\odot$ Sgr A* BH. This is just a rough qualitative sketch of a context, that of the scattering around the MW central MBH, that deserves a much more careful study which we will do in a forthcoming paper.

3.4 Number of ejected stars

After discussing the fate of an individual test star moving circularly around a point like GC, we want here to quantify the actual number of stars belonging to a GC that can become bound to the SMBH or ejected at high velocity or even hypervelocity after the interaction with the SMBH. A suitable estimation comes from the evaluation of the number of stars in nearly circular orbits in a self-consistent model of GC of known distribution function (DF). Of course, the DF is not unique and depends both on the functional form of the GC gravitational potential and on the level of anisotropy. Here we consider two different gravitational potentials for the GC:

(i) a Hernquist potential (Hernquist 1990)

$$\Phi(r) = -\frac{GM}{r+a}, \tag{14}$$

where M is the total GC mass and a its core radius;

(ii) a Plummer potential (Plummer 1911)

$$\Phi(r) = -\frac{GM}{\sqrt{r^2+a^2}}, \tag{15}$$

where, again, M is the total GC mass and a its core radius.

Downloaded from http://mnras.oxfordjournals.org/ at Universita' degli Studi Roma La Sapienza on May 6, 2016

Subsequently, we treated both the isotropic and anisotropic cases. With the usual definition of the anisotropy parameter

$$\beta = 1 - \frac{\sigma_\theta^2 + \sigma_\phi^2}{2\sigma_r^2}, \tag{16}$$

where σ_r, σ_θ and σ_ϕ are the velocity dispersions in spherical polar coordinates, an isotropic model has $\beta = 0$, while β is non-zero for anisotropic cases.

Using different modelizations, we computed the local fraction of stars of the GC on nearly circular orbits, $G(\xi) = \nu_c(\xi)/\nu(\xi)$, as function of $\xi \equiv r/a$, where $\nu(\xi)$ is the local density of bound stars of any velocity, while $\nu_c(\xi)$ is that of stars moving on nearly circular orbit of scaled radius ξ, i.e. those with velocity very close to the local circular velocity $v_c(\xi)$.

For the Hernquist potential,

$$\nu(\xi) = \frac{M}{2\pi a^3}\frac{1}{\xi(1+\xi)^3}, \tag{17}$$

while for the Plummer potential

$$\nu(\xi) = \frac{3M}{4\pi a^3}\frac{1}{(1+\xi^2)^{5/2}}. \tag{18}$$

The function $\nu_c(\xi)$ depends, besides the assumed potential, also on the degree of velocity anisotropy and can be calculated as described in appendix. The resulting $\nu_c(\xi)$ will depend also on the 'tolerance' δ, which quantifies the departure from the exact circular velocity. In our calculations we consider in $\nu_c(\xi)$ all the stars having a local speed in the interval $-\delta \leq v/v_c \leq +\delta$, with $\delta = 0.05$.

As expected, Figs 6(a) and (b) show that the isotropic ($\beta = 0$) model fraction stays between the radially biased ($\beta = +1/2$) and the tangentially biased ($\beta = -1/2$) models.

Combining these evaluations of the local fractional abundance of stars on nearly circular orbits with the branching ratios obtained in the previous sections, we can evaluate the actual numbers of stars which escape from or remain bound to the GC or the SMBH after close GC–SMBH interactions. This requires some assumptions. First of all we assume that the GC is composed by a single-mass ($m_* = 1\ M_\odot$) population of stars. Moreover, we assume that the core radius has a size which is half the innermost circular orbit radius chosen.

The number of stars in nearly circular orbits is evaluated by mean of the integral

$$N_c = 4\pi\mathcal{N}\int_{r_a}^{r_b} \nu_c(r) r^2 \mathrm{d}r, \tag{19}$$

where $\mathcal{N} = 10^4$, 10^5, 10^6 is the assumed number of stars in the GCs, while r_a and r_b are given by

$$r_{a,b} = \frac{GM(r)}{v_{a,b}^2}, \tag{20}$$

being $v_{a,b} = v_c \pm \delta v_c$. A straightforward product of N_c with the fractions of bound to the GC or BH or unbound (high-velocity or hypervelocity) stars, as derived by our scattering experiments presented in the previous sections, gives an estimate of the actual number of stars ejected thanks to the GC–BH interaction mechanism.

Figs 7–9 report the number of stars ejected from the GC after the close interaction between the GC and the BH, as function of the circular orbit radius for various values of α, both in the isotropic ($\beta = 0$) and anisotropic ($\beta = \pm 1/2$) Hernquist and Plummer GC models. The number of ejected stars depends, besides on the GC mass, on the GC potential model and on the degree of anisotropy, as shown by Fig. 6.

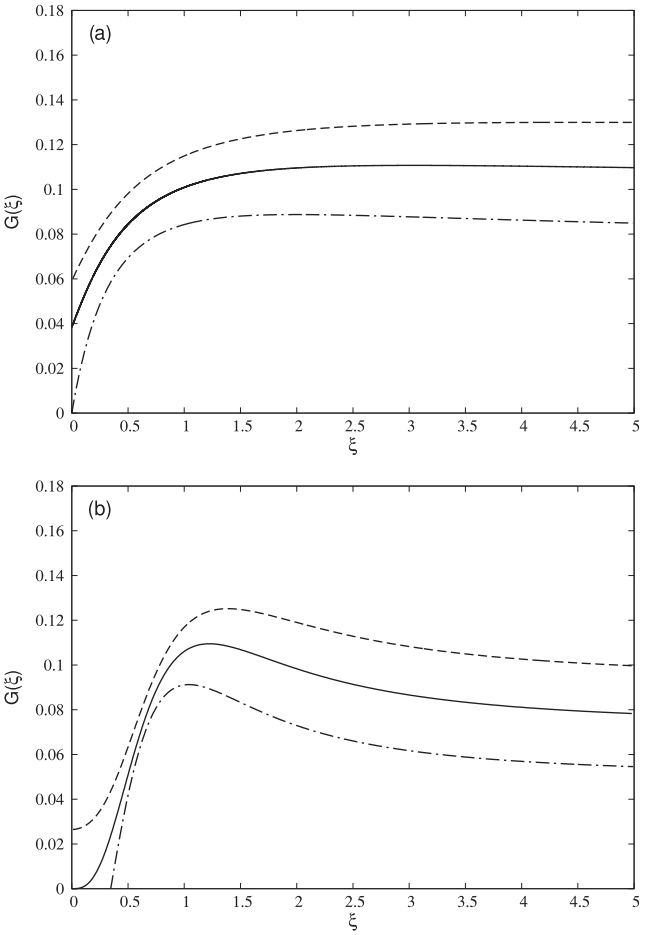

Figure 6. Local fraction $G(\xi) \equiv \nu_c(\xi)/\nu(\xi)$ of stars in nearly circular orbit with $\delta = 0.05$, for the Hernquist (a) and the Plummer (b) potentials. The isotropic fraction ($\beta = 0$, solid line) stands between the tangentially biased fraction ($\beta = -1/2$, dashed line) and the radially biased fraction ($\beta = +1/2$, dot–dashed line).

Moreover, the number of ejected stars increases with the GC mass. Actually this mechanism would produce 10–10^2, 10^2–10^3 and 10^3–10^4 high-velocity stars for GC mass of 10^4, 10^5 and $10^6\ M_\odot$, respectively.

This almost linear dependence of the number of ejected stars on the GC mass is explained by the fact that the gravitational energy per unit mass available to be converted into the test star kinetic energy is linearly scaling with M_{GC}, $E_{gr} \sim M_{GC}$.

The same token holds for an explanation of the isotropic–anisotropic models difference. In the case of tangentially biased models ($\beta = -1/2$) there is a larger fraction of ejected stars because of the larger fraction of stars in nearly circular orbits. On the other hand, the fraction of ejected stars is smaller for radially biased models ($\beta = +1/2$).

4 CONCLUSIONS

The phenomenon of the existence of high-velocity stars, or even HVSs, in our Galaxy has been explained in the literature (Yu & Tremaine 2003) in terms of the presence of a massive BH in the

Downloaded from http://mnras.oxfordjournals.org/ at Universita' degli Studi Roma La Sapienza on May 6, 2016

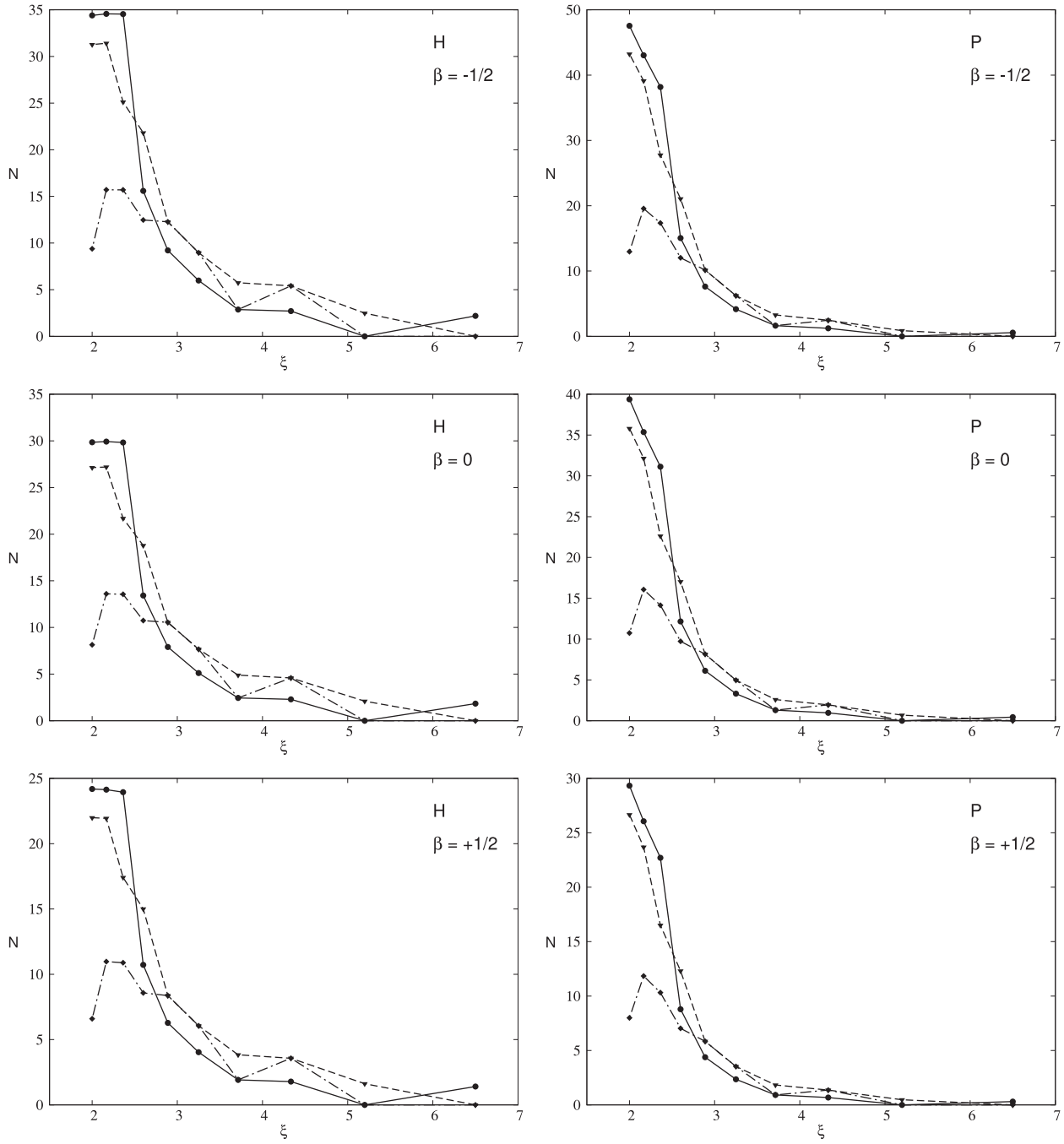

Figure 7. Number of stars ejected by the GC with mass $M_{GC} = 10^4\,M_\odot$ as function of ξ, for Hernquist (left) and Plummer potential (right), for different values of the anisotropy parameter β. The different line styles refer to different GC orbit: $\alpha = 0.1$, solid line; $\alpha = 0.2$, dashed line; $\alpha = 0.3$, dot–dashed line. $\alpha = 0.4$ and 0.5 orbits give no ejected stars.

galactic centre ($\sim 4 \times 10^6\,M_\odot$ in our MW). The mechanism of star acceleration to high speed requires, indeed, an efficient energy exchange in a multiple system, i.e. a three or more bodies interaction with the massive BH (Hills 1988) or, if it exists, with a BH binary (Sesana et al. 2006).

In this paper we deepened what has been recently found by Arca Sedda et al. (in preparation) and preliminarily presented in Spera, Arca-Sedda & Capuzzo-Dolcetta (2015), i.e. that the close passage of a massive GC near a massive BH can be source of ejection of stars from the cluster, which are accelerated to high speeds. In our study, we assumed $M_{BH} = 10^8\,M_\odot$ with the scope of better identifying the actual physical mechanism. The underlying mechanism is likely a three-body interaction, where the 'bodies' are the SMBH ($10^8\,M_\odot$), the GC (10^4, 10^5 and $10^6\,M_\odot$) and the test star ($1\,M_\odot$) belonging to the GC.

We have performed a series of high precision integration of the orbits of such three bodies to check the probability for the test star orbiting a GC, which experiences a close (pericentre distance less than 10 pc) encounter, to remain bound to the cluster, to be captured by the BH or gain high velocity such as to overcome the

Downloaded from http://mnras.oxfordjournals.org/ at Universita' degli Studi Roma La Sapienza on May 6, 2016

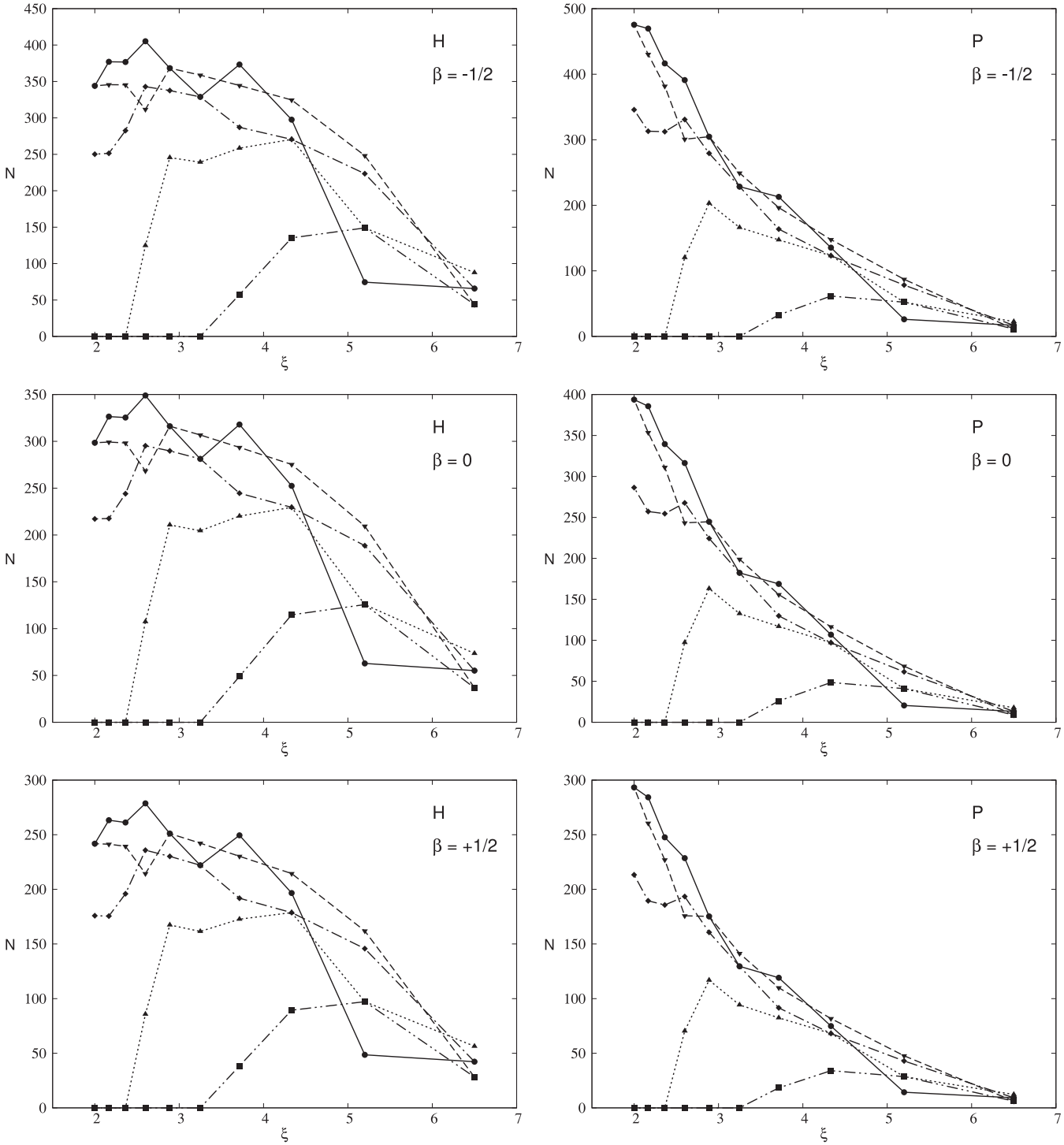

Figure 8. Number of stars ejected by the GC with mass $M_{GC} = 10^5\,M_\odot$ as function of ξ, for Hernquist (left) and Plummer potential (right), for different values of the anisotropy parameter β. The different line styles refer to different GC orbit: $\alpha = 0.1$, solid line; $\alpha = 0.2$, dashed line; $\alpha = 0.3$, dot–dashed line; $\alpha = 0.4$, dotted line; $\alpha = 0.5$, double dot–dashed line.

cluster escape velocity and, possibly, the galaxy escape velocity. We determined the branching ratios of these three phenomena and found the following:

(i) the efficiency of the star acceleration process is almost linear in M_{GC};

(ii) a massive GC (composed by 10^6 identical 1 $M_\odot$ stars) releases, in a single close passage around the SMBH, about 10^4 stars;

(iii) in a very close GC–BH encounter ($M_{GC} = 10^6\,M_\odot, \alpha = 0.1$) the probability of stars to remain bound, become bound to the BH or escape from the cluster are ∼5, ∼45 and ∼50 per cent, respectively;

Downloaded from http://mnras.oxfordjournals.org/ at Universita' degli Studi Roma La Sapienza on May 6, 2016

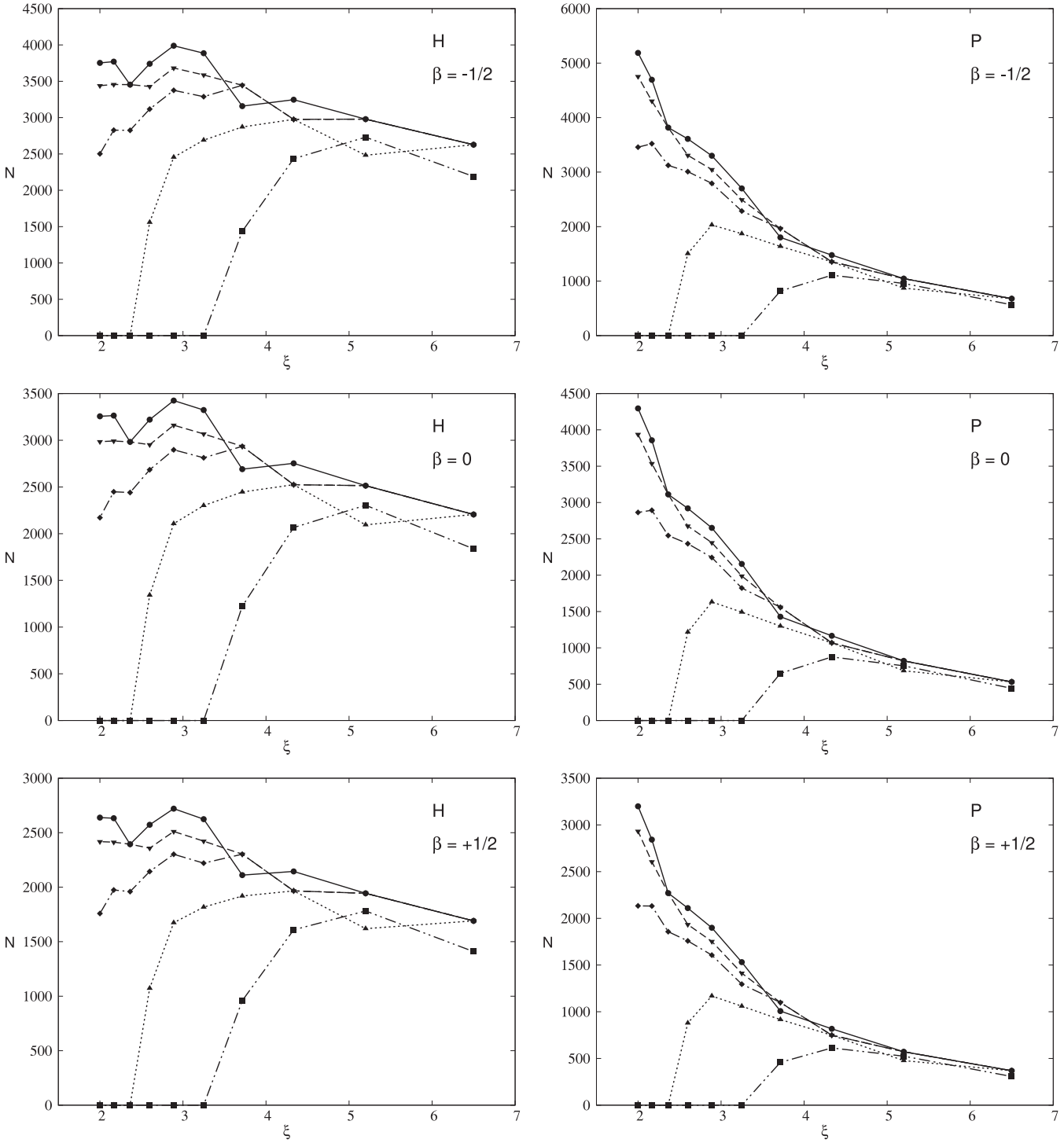

Figure 9. Number of stars ejected by the GC with mass $M_{GC} = 10^6\,M_\odot$ as function of ξ, for Hernquist (left) and Plummer potential (right), for different values of the anisotropy parameter β. The different line styles refer to different GC orbit: $\alpha = 0.1$, solid line; $\alpha = 0.2$, dashed line; $\alpha = 0.3$, dot–dashed line; $\alpha = 0.4$, dotted line; $\alpha = 0.5$, double dot–dashed line.

(iv) the fractions of stars, with respect to the total ejected stars, which escape from the whole galaxy is ∼18 per cent for an $M_{tot} = 7.81 \times 10^{10}\,M_\odot$ elliptical and ∼0.5 per cent for an $M_{tot} = 6.60 \times 10^{11}\,M_\odot$ spiral galaxy.

Moreover, we studied the effects of the inclination of the star initial orbit around the GC with respect to the GC orbit. When the orbits are perpendicular, the branching ratios of the ejected stars and of the stars captured by the BH decrease, while the branching ratio of stars which remain bound to the GC increases. Therefore, the overall effect of the increasing inclination of the star orbit with respect to the GC orbit consists mainly in a slight reduction of the fraction of stars ejected from the GC and/or captured by the BH. Correspondingly, the velocity profile of the ejected stars is peaked at lower velocity values.

Downloaded from http://mnras.oxfordjournals.org/ at Universita' degli Studi Roma La Sapienza on May 6, 2016

Furthermore, we performed the same set of three-body scattering experiments for the $M_{GC} = 10^6$ GC assuming it is a Plummer sphere with a core radius of 0.5 pc. In this smoothed case, the velocity distribution shrinks towards lower values of the velocity since the amount of gravitational energy, to convert into kinetic one, decreases. As a consequence, we found no ejection of HVSs, suggesting that, when the GC is described by a smoothed potential, it is likely to eject only high-velocity stars, which escape the GC–BH system, but still remain bound to the host galaxy.

Different high-velocity and hypervelocity ejection mechanisms predict different spatial distributions, velocity distributions and physical and kinematic characteristics of the ejected stars (Brown 2015).

One important feature of this mechanism is the collimation of the ejected stars. We found that the high-velocity stars are ejected in sort of jets, whose angular amplitude depends on the GC mass. High-velocity stars produced by the interaction of a low-mass GC with a massive BH are likely to be concentrated in a small amplitude jet. On the other hand, higher GC masses make the ejection jets have a huge amplitude and stars are ejected in a nearly isotropic emission. These results are compatible with Sesana et al. (2006) finding. Note that our results refer to a single GC–BH interaction; anyway, we expect a production of a high-velocity star jet every time a GC undergoes a close encounter with a massive BH. Consequently, small clusters of high-velocity stars are expected to be present in the sky, whose characteristics depend strongly on the mass of the GC from which they come from. At this regard, it is interesting to note that about half of the discovered HVSs are clumped around the Leo constellation (Brown et al. 2014). The kinematics and dynamics of the jets, their position in the sky and their velocity profile may give information about the GC–BH interaction that produced them, in particular about the GC mass and its orbits before being disrupted by the massive BH. Moreover, some stars of the jet, the ones on the right tail of the velocity distribution, may have such high velocities to be HVSs, and so to be lost by the jet itself since they are unbound with respect to the hosting galaxy gravitational field. Being composed by stars formerly belonging to a GC, we expect that the jets contains stars of about same age and metallicity, with a common flight time. Hence, in principle, by measuring the dynamical and physical properties of such high-velocity jets, it would be possible to infer information about the GC progenitor before its tidal erosion by the massive BH.

Finally, a counterpart of such jets is the production of a population of stars orbiting the inner galactic regions and which share age and metallicity with the jet stars.

As mentioned above, we assumed $M_{BH} = 10^8\ M_\odot$ with the scope of better identifying the underlying physical mechanism. For what concerns the MW, we expect that the velocity distribution would be peaked at lower velocities due to the less energetic mechanism (the SgrA* mass being a factor 25 lower), with the production of high-velocity rather than hypervelocity stars. However, we suggest that, in the very last, eccentric and narrow GC orbits, some HVSs may be produced through the mechanism studied in this work. Finally, we suggest that the recent observed runaway RR Lyrae variable star, MACHO 176.18833.411, (Kunder et al. 2015) may have been produced through the mechanism studied in this work.

ACKNOWLEDGEMENTS

We thank S. Mikkola for making available to us his ARW code and for useful discussions about his use. We also thank E. M. Rossi for useful discussions about HVSs and the mechanism studied in this work. Finally, we thank the anonymous referee for helpful comments and suggestions on this manuscript.

REFERENCES

Antonini F., Capuzzo-Dolcetta R., Mastrobuono-Battisti A., Merritt D., 2012, ApJ, 750, 111
Baumgardt H., Gualandris A., Portegies Zwart S. F., 2006, J. Phys. Conf. Ser., 54, 301
Binney J., 1981, MNRAS, 196, 455
Binney J., Tremaine S., 2011, Galactic Dynamics. Princeton Univ. Press, Princeton, NJ
Blaauw A., 1961, Bull. Astron. Inst. Neth., 15, 265
Bonanos A. Z., Lopez-Morales M., Hunter I., Ryans R. S. I., 2008, ApJ, 675, L77
Bromley B. C., Kenyon S. J., Geller M. J., Barcikowski E., Brown W. R., Kurtz M. J., 2006, ApJ, 653, 1194
Brown W. R., 2015, ARA&A, 53, 15
Brown W. R., Geller M. J., Kenyon S. J., Kurtz M. J., 2005, ApJ, 622, L33
Brown W. R., Geller M. J., Kenyon S. J., 2009, ApJ, 690, 1639
Brown W. R., Anderson J., Gnedin O. Y., Bond H. E., Geller M. J., Kenyon S. J., Livio M., 2010, ApJ, 719, L23
Brown W. R., Geller M. J., Kenyon S. J., 2014, ApJ, 787, 89
Bulirsch R., Stoer J., 1966, Numer. Math., 8, 1
Capuzzo-Dolcetta R., 1993, ApJ, 415, 616
Capuzzo-Dolcetta R., Miocchi P., 2008, MNRAS, 388, L69
Fujita Y., 2009, ApJ, 691, 1050
Ginsburg I., Loeb A., 2006, MNRAS, 368, 221
Ginsburg I., Loeb A., Wegner G. A., 2012, MNRAS, 423.1, 948
Gnedin O. Y., Gould A., Miralda-Escud J., Zentner A. R., 2005, ApJ, 634, 344
Gould A., Quillen A. C., 2003, ApJ, 592, 935
Gualandris A., Portegies Zwart S. F., 2007, MNRAS, 376, L29
Gualandris A., Portegies Zwart S. F., Sipior M. S., 2005, MNRAS, 363, 223
Gvaramadze V. V., 2009, MNRAS, 395, L85
Gvaramadze V. V., Gualandris A., 2011, MNRAS, 410, 304
Gvaramadze V. V., Gualandris A., Portegies Zwart S. F., 2009, MNRAS, 396, 570
Hansen B. M. S., 2007, ApJ, 671, L133
Hellström C., Mikkola S., 2010, Celest. Mech. Dyn. Astron., 106, 143
Hernquist L., 1990, ApJ, 356, 359
Hills J. G., 1988, Nature, 331, 687
Hoogerwerf R., de Bruijne J. H. J., de Zeeuw P. T., 2001, A&A, 365, 49
Humason M. L., Zwicky F., 1947, ApJ, 105, 85
Kobayashi S., Hainick Y., Sari R., Rossi E. M., 2012, ApJ, 670, 747
Kollmeier J. A., Gould A., Knapp G., Beers T. C., 2009, ApJ, 697, 1543
Kollmeier J. A. et al., 2010, ApJ, 723, 812
Kornreich D. A., Lovelace R. V. E., 2008, ApJ, 681, 104
Kunder A. et al., 2015, ApJ, 808, L12
Leonard P. J. T., Duncan M. J., 1990, AJ, 99, 608
Li Y. et al., 2015, Res. Astron. Astrophys., 15, 1364
Lingam M., 2014, Ap&SS, 354, 561
Loeb A., 2011, J. Cosmol. Astropart. Phys., 2011, 023
Lopez-Morales M., Bonanos A. Z., 2008, ApJ, 685, L47
Marconi A., Hunt L. K., 2003, ApJ, 589, L21
Mikkola S., Aarseth S., 2001, Celest. Mech. Dyn. Astron., 84, 343
Mikkola S., Merritt D., 2006, MNRAS, 372, 219
Mikkola S., Merritt D., 2008, AJ, 135, 2398
Mikkola S., Tanikawa K., 1999a, Celest. Mech. Dyn. Astron., 74, 287
Mikkola S., Tanikawa K., 1999b, MNRAS, 310, 745
Miyamoto M., Nagai R., 1975, PASJ, 27, 533
O'Leary R. M., Loeb A., 2008, MNRAS, 383, 86
Palladino L. E., Schlesinger K. J., Holley-Bockelmann K., Allende Prieto C., Beers T. C., Lee Y. S., Schneider D. P., 2014, ApJ, 780, 7
Perets H. B., 2009, ApJ, 698, 1330
Perets H. B., Subr L., 2012, ApJ, 751, 133

Downloaded from http://mnras.oxfordjournals.org/ at Universita' degli Studi Roma La Sapienza on May 6, 2016

Perets H. B., Hopman C., Alexander T., 2007, ApJ, 656, 709
Plummer H. C., 1911, MNRAS, 71, 140
Portegies Zwart S. F., 2000, ApJ, 544, 437
Poveda A., Ruiz J., Allen C., 1967, Bol. Obs. Tonantzintla Tacubaya, 4, 86
Przybilla N., Nieva M. F., Heber U., Butler K., 2008, ApJ, 684, L103
Rossi E. M., Kobayashi S., Sari R., 2014, ApJ, 795, 125
Rownd B. K., Dickey J. M., Helou G., 1994, AJ, 108, 1638
Sari R., Kobayashi S., Rossi E. M., 2010, ApJ, 708, 605
Scheck L., Kifonidis K., Janka H.-T., Müller E., 2006, A&A, 457, 963
Sesana A., Haardt F., Madau P., 2006, ApJ, 651, 392
Sesana A., Haardt F., Madau P., 2007, MNRAS, 379, L45
Sherwin B., Loeb A., O'Leary R., 2008, MNRAS, 386, 1179
Silva M. D. V., Napiwotzki R., 2011, MNRAS, 411, 2596
Spera M., Arca-Sedda M., Capuzzo-Dolcetta R., 2015, in Spurzem R., Liu F. K., eds, Proc. IAU Symp. 312, Star Clusters and Black Holes in Galaxies and Across Cosmic Time. Cambridge University Press, Cambridge
Szebehely V., 1966, Theory of Orbits. Academic Press, New York
Tutukov A. V., Fedorova A. V., 2009, Astron. Rep., 53, 839
Vickers J. J., Smith M. C., Grebel E. K., 2015, AJ, 150, 77
Wang J. C. L., Sulkanen M. E., Lovelace R. V. E., 1992, ApJ, 390, 46
Yu Q., Madau P., 2007, MNRAS, 379, 1293
Yu Q., Tremaine S., 2003, ApJ, 599, 1129
Zhong J. et al., 2014, ApJ, 789, L2
Zubovas K., Wynn G. A., Gualandris A., 2013, ApJ, 771, 118

APPENDIX A: FRACTION OF PARTICLES IN NEARLY CIRCULAR ORBITS

A spherical stellar system confined by a steady spherical potential $\Phi(r)$ can be described by a unique ergodic DF. The DF depends on the phase-space coordinates only through the Hamiltonian $H(\boldsymbol{r}, \boldsymbol{v}) = \frac{1}{2}v^2 + \Phi(\boldsymbol{r})$ (Binney & Tremaine 2011) and can be written as a non-negative $f(\mathcal{E})$, where $\mathcal{E} = -H + \Phi_0$ is the *relative* energy, with Φ_0 a constant chosen such that $f > 0$ for $\mathcal{E} > 0$ and $f = 0$ for $\mathcal{E} \leq 0$.

The functional expression of $f(\mathcal{E})$, which obviously depends on the functional form of $\Phi(r)$, can be found by the Eddington's inversion formula

$$f(\mathcal{E}) = \frac{1}{\sqrt{8}\pi^2}\left[\int_0^{\mathcal{E}} \frac{\mathrm{d}\Psi}{\sqrt{\mathcal{E}-\Psi}}\frac{\mathrm{d}^2\nu}{\mathrm{d}\Psi^2} + \frac{1}{\sqrt{\mathcal{E}}}\left(\frac{\mathrm{d}\nu}{\mathrm{d}\Psi}\right)\Big|_{\Psi=0}\right], \quad \text{(A1)}$$

where $\nu(\boldsymbol{r})$ is the spatial number density generated by the DF

$$\nu(\boldsymbol{r}) = \int \mathrm{d}^3\boldsymbol{v} f(\boldsymbol{r}, \boldsymbol{v}) = 4\pi \int_0^{\sqrt{2\Psi}} \mathrm{d}v\, v^2 f(\Psi - \frac{1}{2}v^2), \quad \text{(A2)}$$

and where $\Psi = -\Phi + \Phi_0$.

The Hernquist potential (Hernquist 1990), for which $\Phi_0 = \Phi(r \to \infty) = 0$,

$$\Phi(r) = -\frac{GM}{r+a}, \quad \text{(A3)}$$

where M is the total mass and a is the core radius, leads, by equation (A1), to

$$f(\mathcal{E}) = \frac{1}{\sqrt{2}(2\pi)^3(GMa)^(3/2)}\frac{\sqrt{\widetilde{\mathcal{E}}}}{(1-\widetilde{\mathcal{E}})^2} \times \left[(1-2\widetilde{\mathcal{E}})(8\widetilde{\mathcal{E}}^2 - 8\widetilde{\mathcal{E}} - 3) + \frac{3\arcsin\sqrt{\widetilde{\mathcal{E}}}}{\sqrt{\widetilde{\mathcal{E}}(1-\widetilde{\mathcal{E}})}}\right], \quad \text{(A4)}$$

where $\widetilde{\mathcal{E}} = \mathcal{E}/(GM/a)$ is the adimensional relative energy. The Plummer potential (Plummer 1911), for which $\Phi_0 = \Phi(r \to \infty) = 0$,

$$\Phi(r) = -\frac{GM}{\sqrt{r^2+a^2}}, \quad \text{(A5)}$$

where, again, M is the total mass and a is the core radius, leads, by equation (A1), to

$$f(\mathcal{E}) = \frac{96\widetilde{\mathcal{E}}^{7/2}}{7\sqrt{8}\pi^3(GMa)^(3/2)}, \quad \text{(A6)}$$

where $\widetilde{\mathcal{E}}$ is, again, the adimensional relative energy.

The above DFs are isotropic, i.e. the anisotropy parameter

$$\beta = 1 - \frac{\sigma_\theta^2 + \sigma_\phi^2}{2\sigma_r^2}, \quad \text{(A7)}$$

is null. In equation (A7), σ_r, σ_θ and σ_ϕ are the velocity dispersions on the r, θ and ϕ component, respectively, in a spherical polar reference frame.

Models with $\beta \neq 0$ can be generated by taking the DF in the form (Binney & Tremaine 2011)

$$f(\mathcal{E}, L) = L^{-2\beta} f_1(\mathcal{E}). \quad \text{(A8)}$$

In equation (A8), L is the absolute value of the specific angular momentum and $f_1(\mathcal{E})$ is an arbitrary non-negative function of $\mathcal{E}$. Given the DF in the form of equation (A8), the space number density is given by

$$\nu(\boldsymbol{r}) = \int \mathrm{d}^3\boldsymbol{v} f(\boldsymbol{r}, \boldsymbol{v}) = = 2\pi \int_0^{\pi} \mathrm{d}\eta\, \sin\eta \int_0^{\sqrt{2\Psi}} \mathrm{d}v\, v^2 f(\Psi - \frac{1}{2}v^2, rv\sin\eta). \quad \text{(A9)}$$

The expression of $f_1(\mathcal{E})$ depends on the form of the potential $\Phi(r)$ and on the value of the anisotropy parameter β. In the case $\beta = +1/2$, the expression of $f_1(\mathcal{E})$ is given by

$$f_1(\mathcal{E}) = \frac{1}{2\pi^2}\frac{\mathrm{d}}{\mathrm{d}\Psi}(r\nu)\Big|_{\Psi=\mathcal{E}}, \quad \text{(A10)}$$

while in the case $\beta = -1/2$ by

$$f_1(\mathcal{E}) = \frac{1}{2\pi^2}\frac{\mathrm{d}^2}{\mathrm{d}\Psi^2}(\nu/r)\Big|_{\Psi=\mathcal{E}}. \quad \text{(A11)}$$

In the case of the Hernquist potential (A3) we thus have

$$f_1(\widetilde{\mathcal{E}}) = \frac{3\widetilde{\mathcal{E}}}{4\pi^3 GMa}, \quad \text{(A12)}$$

for $\beta = +1/2$, and

$$f_1(\widetilde{\mathcal{E}}) = \frac{1}{2\pi^3(GMa)^2}\frac{\widetilde{\mathcal{E}}^5 - 10\widetilde{\mathcal{E}}^4 + 10\widetilde{\mathcal{E}}^3}{1-\widetilde{\mathcal{E}}^4}, \quad \text{(A13)}$$

for $\beta = -1/2$.

The Plummer potential (A5), instead, leads to

$$f_1(\widetilde{\mathcal{E}}) = \frac{3}{8\pi^3 GMb}\frac{4\widetilde{\mathcal{E}}^3 - 5\widetilde{\mathcal{E}}^5}{(1-\widetilde{\mathcal{E}}^2)^{1/2}}, \quad \text{(A14)}$$

for $\beta = +1/2$, and to

$$f_1(\widetilde{\mathcal{E}}) = \frac{3}{8\pi^3(GMb)^2}\frac{30\widetilde{\mathcal{E}}^4 - 47\widetilde{\mathcal{E}}^6 + 20\widetilde{\mathcal{E}}^8}{(1-\widetilde{\mathcal{E}}^2)^{1/2}}, \quad \text{(A15)}$$

for $\beta = -1/2$.

Downloaded from http://mnras.oxfordjournals.org/ at Universita' degli Studi Roma La Sapienza on May 6, 2016

Finally, to calculate the fraction of stars on nearly circular orbits $G(\xi) = v_c(\xi)/v(\xi)$, we consider a 'tolerance' δ, which quantifies the departure from the exact circular velocity. In our calculations we consider in $v_c(\xi)$ all the stars having a local speed in the interval $-\delta \leq v/v_c \leq +\delta$. Consequently, their number density is given by

$$v_c(\boldsymbol{r}) = \int \mathrm{d}^3\boldsymbol{v}\, f(\boldsymbol{r}, \boldsymbol{v}) = \\ = I_\beta \int_{v_c-\delta v_c}^{v_c+\delta v_c} \mathrm{d}v\; v^2 f(\Psi - \frac{1}{2}v^2, rv\sin\eta), \tag{A16}$$

where

$$I_\beta = \begin{cases} 4\pi & \beta = 0 \\ 2\pi \int_0^\pi \mathrm{d}\eta\; \sin\eta & \beta = \pm 1/2. \end{cases} \tag{A17}$$

This paper has been typeset from a TEX/LATEX file prepared by the author.

Downloaded from http://mnras.oxfordjournals.org/ at Universita' degli Studi Roma La Sapienza on May 6, 2016